POLITECNICO DI TORINO
Repository ISTITUZIONALE

Magnetic and Combined Field Integral Equations Based on the Quasi-Helmholtz Projectors

(Article begins on next page)

12 September 2024

Magnetic and Combined Field Integral Equations Based on the Quasi-Helmholtz Projectors

Adrien Merlini, *Student Member, IEEE*, Yves Beghein, Kristof Cools, Eric Michielssen, *Fellow, IEEE*, and Francesco P. Andriulli, *Senior Member, IEEE*

Abstract—Boundary integral equation methods for analyzing electromagnetic scattering phenomena typically suffer from several of the following shortcomings: (i) ill-conditioning when the frequency is low; (ii) ill-conditioning when the discretization density is high; (iii) ill-conditioning when the structure contains global loops (which are computationally expensive to detect); (iv) incorrect solution at low frequencies due to a loss of significant digits; (v) presence of spurious resonances. In this paper, quasi-Helmholtz projectors are leveraged to obtain a magnetic field integral equation (MFIE) that is immune to drawbacks (i)-(iv). Moreover, when this new MFIE is combined with a regularized electric field integral equation (EFIE), a new quasi-Helmholtz projector combined field integral equation (CFIE) is obtained that also is immune to (v). Numerical results corroborate the theory and show the practical impact of the newly proposed formulations.

Index Terms—Electric, Magnetic, and Combined Field Integral Equations, Preconditioning, Calderon strategies.

I. INTRODUCTION

TIME-HARMONIC scattering by perfect electrically conducting (PEC) objects oftentimes is modeled using frequency domain boundary integral equations. Among them, electric and magnetic field integral equations (EFIE and MFIE) [1], [2] are the most popular.

Although the EFIE is easily discretized using Rao-Wilton-Glisson (RWG) basis functions [3], it suffers from ill-conditioning when the frequency is low and/or the discretization density is high. The MFIE, on the other hand, remains well-conditioned in both regimes, provided that a mixed discretization scheme is employed [4]. In practice, however, it is not feasible to obtain accurate results for the MFIE at extremely low frequencies without resorting to highly precise numerical quadrature methods. Even at moderately low frequencies, both the EFIE and MFIE suffer from a loss of significant digits in the non-solenoidal part of the current [5]–[7]. This loss of significant digits in the current is caused by the storage of two very differently scaled floating point numbers in the same memory location. This results in many digits of

the smaller number to fall below the numerical cutoff imposed by the larger number.

The EFIE's low-frequency conditioning and loss of accuracy problems can be overcome by using loop-star or loop-tree decompositions [8]–[12]. For multiply connected geometries, this requires the detection of global loops, which is computationally expensive [8]. These techniques also fail to address dense discretization breakdown phenomena [13], [14] that causes the EFIE's condition number to grow quadratically with the inverse of the average edge length. Worse still, loop-star techniques for combatting the EFIE's low-frequency conditioning problems further degrade the equation's dense discretization behavior [15].

Several formulations have been introduced to address the EFIE's low-frequency breakdown without resorting to global loop detection [16]–[18]. These solutions, however, do not address the equation's ill-conditioning due to dense discretization. Both issues can be concurrently tackled by leveraging hierarchical quasi-Helmholtz decompositions [13], [19]–[21]. Approaches based on Calderón preconditioning [22]–[27] and Debye-inspired schemes [28] have been successfully coupled with these decompositions [14], [29]–[31]. The price to be paid for this dual stabilization is, once again, the need for global loop detection at very low frequencies. In addition, several of the aforementioned techniques fail to properly address low-frequency loss of significant digits occurring in the solution vector [5], [6], [32], [33]. Several of the above drawbacks have been successfully addressed by the promising scheme in [34] which introduces decoupled vector and scalar potentials obtained by exploiting freedom in the choice of the gauge to obtain a stable formulation. Alternative remedies to the loss of significant digits include perturbation methods [5], [32], [35] and Calderón regularization combined with loop-star decompositions [30], [31]. Both families of solutions do, however, have shortcomings: the former is only applicable at low frequencies and exhibits the same spectral issues as the formulation it is applied to – dense discretization breakdown for the EFIE or global loop detection for the MFIE and Calderón EFIE – while the latter also requires global loop detection and treatment of the dense discretization instability of the loop-star decomposition. It should also be noted that some recent incarnations of augmented equations are immune to several of the above mentioned drawbacks, though they require the recovery of auxiliary quantities [36], [37].

Recently, an electric type equation based on quasi-Helmholtz projectors was proposed that is immune to all of the aforementioned issues [38]. A similar regularization has also

A. Merlini is with the Department of Electronics and Telecommunications of Politecnico di Torino, Turin, Italy (e-mail: adrien.merlini@polito.it).

Y. Beghein is with the Department of Information Technology (INTEC), Ghent University, 9502 Ghent, Belgium.

K. Cools is with the Department of Electrical Engineering, Delft University of Technology, Delft, Netherlands

E. Michielssen is with the Department of Electrical Engineering and Computer Science, University of Michigan, Ann Arbor, MI 48109, USA (e-mail: emichiel@umich.edu).

F. P. Andriulli is with the Department of Electronics and Telecommunications of Politecnico di Torino, Turin, Italy (e-mail: francesco.andriulli@polito.it).

been applied to the time domain electric field integral equation [39], [40] and both the time domain and the frequency domain PMCHWT equations [41], [42]. Quasi-Helmholtz projectors also have been combined with other integral formulations. For instance, they have been used to cure ill-conditioning in the volume EFIE related to the choice of material parameters [43].

In this paper, quasi-Helmholtz projectors are used to obtain a new MFIE that no longer requires interaction integrals to be computed using extremely accurate quadrature rules. Additionally, the solenoidal (divergence free) and non-solenoidal (non divergence free) current components are scaled such that the loss of significant digits at low frequencies is avoided. As a result, the formulation remains accurate down to extremely low frequencies. Scattering problems involving closed PEC objects can also be solved using the combined field integral equation (CFIE), which is a linear combination of the EFIE and the MFIE. This equation has the added benefit that it does not support spurious resonances [44]. In this paper, the new regularization method for the MFIE is combined with that for the EFIE presented in [38]. The resulting CFIE is not only low-frequency stable but also immune to spurious resonances. Preliminary results of this research have been presented as conference contributions [45], [46]; these publications, however, presented only partial results without proofs and lacked the theoretical apparatus together with all implementation details.

This paper is organized as follows. Section II defines the standard EFIE and MFIE as well as their discretizations and related quasi-Helmholtz current decompositions. Section III applies a quasi-Helmholtz decomposition to a new Calderón-like form of the MFIE. The resulting equation can be discretized accurately using standard numerical quadrature methods, and scaled w.r.t frequency such that no low frequency loss of significance occurs. Section IV combines this new MFIE with the regularized EFIE [38] to obtain an extremely low frequency stable CFIE. Section V discusses numerical results that corroborate the theory and conclusions are presented in Section VI.

II. Background and Notations

The EFIE and MFIE operators $\mathcal{T}_k$ and $\mathcal{K}_k$ are defined as

$$\begin{align}
(\mathcal{T}_k \boldsymbol{j})(\boldsymbol{r}) &= (\mathcal{T}_{\mathrm{s},k}\boldsymbol{j})(\boldsymbol{r}) + (\mathcal{T}_{\mathrm{h},k}\boldsymbol{j})(\boldsymbol{r}), & (1)\\
(\mathcal{T}_{\mathrm{s},k}\boldsymbol{j})(\boldsymbol{r}) &= \mathrm{j}k\eta\hat{\boldsymbol{n}}\times\int_\Gamma \frac{\mathrm{e}^{-\mathrm{j}kR}}{4\pi R}\boldsymbol{j}(\boldsymbol{r}')\mathrm{d}s', & (2)\\
(\mathcal{T}_{\mathrm{h},k}\boldsymbol{j})(\boldsymbol{r}) &= -\frac{\eta}{\mathrm{j}k}\hat{\boldsymbol{n}}\times\nabla\int_\Gamma \frac{\mathrm{e}^{-\mathrm{j}kR}}{4\pi R}\nabla'\cdot\boldsymbol{j}(\boldsymbol{r}')\mathrm{d}s', & (3)\\
(\mathcal{K}_k\boldsymbol{j})(\boldsymbol{r}) &= -\hat{\boldsymbol{n}}\times p.v.\int_\Gamma \nabla\times\frac{\mathrm{e}^{-\mathrm{j}kR}}{4\pi R}\boldsymbol{j}(\boldsymbol{r}')\mathrm{d}s', & (4)
\end{align}$$

where $R = \|\boldsymbol{r}-\boldsymbol{r}'\|$, Γ is the boundary of a closed domain $\Omega \subset \mathbb{R}^3$ and $\hat{\boldsymbol{n}}$ is its exterior normal vector. Furthermore, given the angular frequency ω, $k = \omega\sqrt{\mu\epsilon}$ and $\eta = \sqrt{\mu/\epsilon}$; here ϵ and μ the permittivity and permeability of vacuum, respectively. If Ω is perfectly conducting, it supports an electric current $\boldsymbol{j}(\boldsymbol{r})$ satisfying both the EFIE

$$(\mathcal{T}_k\boldsymbol{j})(\boldsymbol{r}) = \hat{\boldsymbol{n}}\times\boldsymbol{E}^i(\boldsymbol{r}) \qquad (5)$$

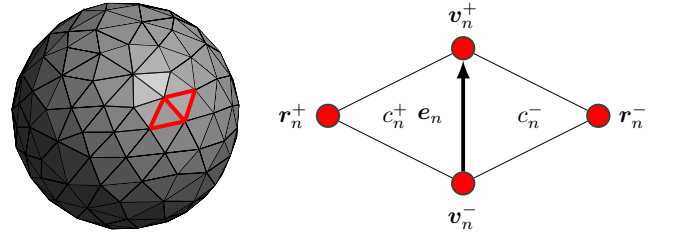

Figure 1. Notations used for the definition of an RWG basis function; $\boldsymbol{e}_n$ denotes the defining inner edge that links vertices $\boldsymbol{v}_n^+$ and $\boldsymbol{v}_n^-$ and c_n^+ and c_n^- the two triangles (cells) connected to this edge which are completed by the vertices $\boldsymbol{r}_n^+$ and $\boldsymbol{r}_n^-$, respectively.

and the MFIE

$$\left(\left(\frac{\mathcal{I}}{2}+\mathcal{K}_k\right)\boldsymbol{j}\right)(\boldsymbol{r}) = \hat{\boldsymbol{n}}\times\boldsymbol{H}^i(\boldsymbol{r}) \qquad (6)$$

for all $\boldsymbol{r}\in\Gamma$; here $\mathcal{I}$ is the identity operator and $\boldsymbol{E}^i$ and $\boldsymbol{H}^i$ denote the impinging electric and magnetic fields, respectively. To numerically solve these equations via a Petrov-Galerkin procedure, $\boldsymbol{j}(\boldsymbol{r})$ is expanded into RWG basis functions $\{\boldsymbol{f}_j(\boldsymbol{r})\}$ [3] as

$$\boldsymbol{j}(\boldsymbol{r}) \approx \sum_{j=1}^{N_e}[\boldsymbol{j}]_j\,\boldsymbol{f}_j(\boldsymbol{r}), \qquad (7)$$

where N_e is the number of edges of the mesh. Following [38], the RWG functions are normalized such that the flux through their defining edges equals one (i.e. they are not normalized by their edge length). Next, the EFIE (5) is tested with rotated RWG functions $\{\hat{\boldsymbol{n}}\times\boldsymbol{f}_i(\boldsymbol{r})\}$, while the MFIE (6) is tested with rotated Buffa-Christiansen (BC) functions [47] $\{\hat{\boldsymbol{n}}\times\boldsymbol{g}_i(\boldsymbol{r})\}$. The BC functions $\{\boldsymbol{g}_j\}$ are divergence-conforming functions defined on the barycentric refinement of the mesh. In addition, they are quasi curl-conforming in the sense that the mixed Gram matrix between curl-conforming rotated BC functions and RWG functions is well-conditioned. For an explicit definition of these functions the reader is referred to [14], [47]. The testing procedure results in the following matrix equations:

$$\boldsymbol{T}\boldsymbol{j} = (\boldsymbol{T}_{\mathrm{s}}+\boldsymbol{T}_{\mathrm{h}})\boldsymbol{j} = \boldsymbol{v}_e, \qquad (8)$$

$$\left(\frac{\boldsymbol{G}^{\mathrm{T}}}{2}+\boldsymbol{K}_k\right)\boldsymbol{j} = \boldsymbol{v}_h, \qquad (9)$$

where

$$\begin{align}
[\boldsymbol{T}]_{ij} &= (\hat{\boldsymbol{n}}\times\boldsymbol{f}_i, \mathcal{T}_k\boldsymbol{f}_j), & (10)\\
[\boldsymbol{T}_{\mathrm{s}}]_{ij} &= (\hat{\boldsymbol{n}}\times\boldsymbol{f}_i, \mathcal{T}_{\mathrm{s},k}\boldsymbol{f}_j), & (11)\\
[\boldsymbol{T}_{\mathrm{h}}]_{ij} &= (\hat{\boldsymbol{n}}\times\boldsymbol{f}_i, \mathcal{T}_{\mathrm{h},k}\boldsymbol{f}_j), & (12)\\
[\boldsymbol{K}_k]_{ij} &= (\hat{\boldsymbol{n}}\times\boldsymbol{g}_i, \mathcal{K}_k\boldsymbol{f}_j), & (13)\\
[\boldsymbol{G}]_{ij} &= (\boldsymbol{f}_i, \hat{\boldsymbol{n}}\times\boldsymbol{g}_j), & (14)\\
[\boldsymbol{v}_e]_i &= (\hat{\boldsymbol{n}}\times\boldsymbol{f}_i, \hat{\boldsymbol{n}}\times\boldsymbol{E}^i), & (15)\\
[\boldsymbol{v}_h]_i &= (\hat{\boldsymbol{n}}\times\boldsymbol{g}_i, \hat{\boldsymbol{n}}\times\boldsymbol{H}^i), & (16)
\end{align}$$

with $(\boldsymbol{a},\boldsymbol{b}) = \int_\Gamma \boldsymbol{a}(\boldsymbol{r})\cdot\boldsymbol{b}(\boldsymbol{r})\mathrm{d}s$. In what follows, we denote by $\mathbb{T}$, $\mathbb{T}_s$ and $\mathbb{T}_h$ the BC-expanded counterparts of the discretized operators $\boldsymbol{T}$, $\boldsymbol{T}_{\mathrm{s}}$ and $\boldsymbol{T}_{\mathrm{h}}$, tested with rotated BC

functions and computed with the complex wavenumber $-\mathrm{j}k$. This choice, as further explained in the following, will play a key role in characterizing the high frequency behavior of the final equation.

The solutions of (8) and (9) can be expressed as linear combinations of divergence free (loop and harmonic functions) and of non-divergence free (star functions) components via a quasi-Helmholtz decomposition

$$j = \boldsymbol{\Lambda} l + \boldsymbol{\Sigma} s + \boldsymbol{H} h \qquad (17)$$

where the first two matrices $\boldsymbol{\Lambda} \in \mathbb{R}^{N_e \times N_v}$ and $\boldsymbol{\Sigma} \in \mathbb{R}^{N_e \times N_c}$ represent mappings from the RWG subspace to the local loop and star subspaces, respectively. Here, N_v and N_c are the number of vertices and cells of the mesh, respectively [8], [48]. These two mappings can be defined using only the connectivity information of the discretized geometry as

$$[\boldsymbol{\Lambda}]_{ij} = \begin{cases} 1 & \text{if vertex } j \text{ equals } \boldsymbol{v}_i^+ \\ -1 & \text{if vertex } j \text{ equals } \boldsymbol{v}_i^- \\ 0 & \text{otherwise} \end{cases} \qquad (18)$$

and

$$[\boldsymbol{\Sigma}]_{ij} = \begin{cases} 1 & \text{if the cell } j \text{ equals } c_i^+ \\ -1 & \text{if the cell } j \text{ equals } c_i^- \\ 0 & \text{otherwise}, \end{cases} \qquad (19)$$

where vertices $\boldsymbol{v}_i^-$ and $\boldsymbol{v}_i^+$ define the oriented edge characterizing RWG function i, and c_i^- and c_i^+ denote the corresponding cells (Figure 1). The matrix $\boldsymbol{H}$ represents the mapping from the RWG space to the quasi-harmonic or *global loop* space composed of $2N_h$ functions, where N_h is the number of handles in the structure. The number of handles (or genus) of a surface is its number of holes; a sphere has no handles, while a torus has exactly one. For a complete description of this mapping and the associated harmonic functions, the reader is referred to [8] and [48].

A few properties of these matrices are recalled to facilitate further developments. For the sake of simplicity we restrict ourselves to geometries with a single closed connected component, i.e. a single object containing no apertures. All derivations below can be extended to arbitrary geometries using the relations in [49]. Given this assumption, $\boldsymbol{\Lambda}$ has a null-space spanned by the all-one vector $\mathbf{1}^{\boldsymbol{\Lambda}} \in \mathbb{R}^{N_v}$, i.e.

$$\boldsymbol{\Lambda} \mathbf{1}^{\boldsymbol{\Lambda}} = \mathbf{0}. \qquad (20)$$

Similarly, the linear dependency of the star functions causes $\boldsymbol{\Sigma}$ to exhibit a one-dimensional null-space spanned by the all-one vector $\mathbf{1}^{\boldsymbol{\Sigma}} \in \mathbb{R}^{N_c}$, i.e.

$$\boldsymbol{\Sigma} \mathbf{1}^{\boldsymbol{\Sigma}} = \mathbf{0}. \qquad (21)$$

Finally, it is trivial to show that the loop and star subspaces are orthogonal, i.e.

$$\boldsymbol{\Sigma}^{\mathrm{T}} \boldsymbol{\Lambda} = \mathbf{0}. \qquad (22)$$

As $\boldsymbol{\Lambda}$ and $\boldsymbol{\Sigma}$ are ill-conditioned and because of the high computational cost of detecting global loops required to build $\boldsymbol{H}$, it is convenient to leverage the quasi-Helmholtz projectors

introduced in [38] to obtain a quasi-Helmholtz decomposition of the EFIE and MFIE operators. The projectors are defined as

$$\boldsymbol{P}^{\boldsymbol{\Sigma}} = \boldsymbol{\Sigma} \left(\boldsymbol{\Sigma}^{\mathrm{T}} \boldsymbol{\Sigma} \right)^+ \boldsymbol{\Sigma}^{\mathrm{T}}, \qquad (23)$$
$$\boldsymbol{P}^{\boldsymbol{\Lambda H}} = \mathrm{I} - \boldsymbol{P}^{\boldsymbol{\Sigma}}, \qquad (24)$$

where $^+$ denotes the Moore-Penrose pseudo-inverse and I is the discretized identity operator. Any RWG expansion coefficient vector can then be decomposed as

$$j = \left(\boldsymbol{P}^{\boldsymbol{\Lambda H}} j \right) + \left(\boldsymbol{P}^{\boldsymbol{\Sigma}} j \right) \qquad (25)$$

where $\boldsymbol{P}^{\boldsymbol{\Lambda H}} j$ and $\boldsymbol{P}^{\boldsymbol{\Sigma}} j$ contain the RWG expansions of the solenoidal (loop) and non-solenoidal (star) components of the current, respectively. The solenoidal components of the current are divergence-free functions that form loops, while the non-solenoidal components are their complement and have been shown to be star-like in nature [9]. These projector matrices are Hermitian and also can be used to decompose the RWG testing space. Similarly, the dual projectors $\mathbb{P}^{\boldsymbol{\Lambda}}$ and $\mathbb{P}^{\boldsymbol{\Sigma H}}$, defined as

$$\mathbb{P}^{\boldsymbol{\Lambda}} = \boldsymbol{\Lambda} \left(\boldsymbol{\Lambda}^{\mathrm{T}} \boldsymbol{\Lambda} \right)^+ \boldsymbol{\Lambda}^{\mathrm{T}}, \qquad (26)$$
$$\mathbb{P}^{\boldsymbol{\Sigma H}} = \mathrm{I} - \mathbb{P}^{\boldsymbol{\Lambda}}, \qquad (27)$$

and decompose any linear combination of BC (basis or testing) functions into a non-solenoidal and solenoidal part, respectively. It should be noted that construction of these projectors does not require the detection of global loops, and that $\left(\boldsymbol{\Sigma}^{\mathrm{T}} \boldsymbol{\Sigma} \right)^+$ can be efficiently computed using multigrid preconditioners [38], [50].

III. REGULARIZING THE MFIE AT EXTREMELY LOW FREQUENCIES

A. Low Frequency Behavior of the MFIE

The standard RWG discretization of the MFIE fails to provide accurate results at low frequencies due to the unphysical scaling of the solenoidal and non-solenoidal components of the current [5]. It was shown in [4], [51] that the mixed discretization of the MFIE (in which rotated BC or Chen-Wilton (CW) functions [52] are used as testing functions) improves the accuracy of its solution. In particular, the solenoidal and non-solenoidal components of the current obtained from this formulation scale physically [33]. This result also holds true for multiply connected geometries [53].

The mixed MFIE formulation still suffers from three problems. First, the physical scaling of the current can only be retrieved when interaction integrals are computed to high accuracy [33]. Second, the non-solenoidal current component scales as $\mathcal{O}(\omega)$ whereas the solenoidal component is of $\mathcal{O}(1)$. As a result, at very low frequencies and when using finite precision, both components should be stored in different arrays to prevent the non-solenoidal component from losing accuracy [5], [6], [32], [53], [54]. Third, the static MFIE ($\omega = 0$) has a null space when applied to multiply connected geometries. It follows that the discretized MFIE has N_h singular values that scale as $\mathcal{O}(\omega^2)$ [48]. Any accurate discretization of the MFIE operator must preserve this null-space. Standard RWG discretizations of the MFIE operators are not capable of

correctly modelling this null space [45]. The mixed MFIE, on the other hand, correctly models this null-space in infinite precision. However, after discretization, the null-space associated singular values will not be more accurate than the precision of the quadrature rule.

B. A Robust MFIE Formulation

To address the above MFIE deficiencies we propose the following Calderón-like MFIE:

$$\left(\frac{\mathcal{I}}{2} - \mathcal{K}_{-jk}\right)\left(\frac{\mathcal{I}}{2} + \mathcal{K}_k\right)(j) = \left(\frac{\mathcal{I}}{2} - \mathcal{K}_{-jk}\right)\left(\hat{n}_r \times H^i\right),$$
(28)

where $\mathcal{K}_{-jk}$ is the $\mathcal{K}$ operator computed with the imaginary wavenumber $-jk$ ($k \to -jk$). This equation is the magnetic field counterpart of the (localized) Calderón preconditioned electric operator in [38]. We propose to discretize (28) as

$$\mathbb{O}i = \mathbb{M}^{\mathrm{T}}\left(\frac{G^{\mathrm{T}}}{2} - K_{-jk}\right)\left(G^{\mathrm{T}}\right)^{-1} v_h$$
(29)

where

$$O = \mathbb{M}^{\mathrm{T}}\left(\frac{G^{\mathrm{T}}}{2} - K_{-jk}\right)\left(G^{\mathrm{T}}\right)^{-1}\left(\frac{G^{\mathrm{T}}}{2} + K_k\right)M i,$$
(30)

$$M = P^{\Lambda H}\frac{1}{\alpha} + jP^{\Sigma}\alpha,$$
(31)

$$\mathbb{M} = \mathbb{P}^{\Sigma H}\frac{1}{\alpha} + j\mathbb{P}^{\Lambda}\alpha,$$
(32)

and $M i = j$. The imaginary constant in the definition of M and $\mathbb{M}$ permits the preservation of the relevant parts of the solution for a large class of excitations; see [38].

The coefficient α allows for re-scaling of the solenoidal and non-solenoidal components of the solution i of (29) to prevent loss of significant digits. Because $P^{\Sigma} + P^{\Lambda H} = \mathbb{P}^{\Lambda} + \mathbb{P}^{\Sigma H} = \mathrm{I}$, the operator O in (29) can be decomposed as

$$O = (\mathbb{P}^{\Lambda} + \mathbb{P}^{\Sigma H})O(P^{\Sigma} + P^{\Lambda H}) =$$
$$\mathbb{P}^{\Lambda}OP^{\Sigma} + \mathbb{P}^{\Lambda}OP^{\Lambda H} + \mathbb{P}^{\Sigma H}OP^{\Sigma} + \mathbb{P}^{\Sigma H}OP^{\Lambda H},$$
(33)

which allows for the study of the low-frequency behavior of each of the separate terms. Analysis of the frequency behavior of the first three terms is quite straightforward and yields

$$\mathbb{P}^{\Lambda}OP^{\Sigma} = \mathcal{O}(\alpha^2) \quad k \to 0,$$
(34a)
$$\mathbb{P}^{\Lambda}OP^{\Lambda H} = \mathcal{O}(1) \quad k \to 0,$$
(34b)
$$\mathbb{P}^{\Sigma H}OP^{\Sigma} = \mathcal{O}(1) \quad k \to 0.$$
(34c)

Analysis of the last term in (33) requires special care. It is known that when decomposing K_k as

$$K_k = K_0 + K_k',$$
(35)

where K_0 is the static limit of K_k and $K_k' = K_k - K_0$ is the dynamic remainder, $K_k' = \mathcal{O}(k^2)$ as $k \to 0$ [53]. When using this decomposition in (29), it can be verified that K_0 satisfies

$$\mathbb{P}^{\Sigma H}\left(\frac{G^{\mathrm{T}}}{2} - K_0\right)\left(G^{\mathrm{T}}\right)^{-1}\left(\frac{G^{\mathrm{T}}}{2} + K_0\right)P^{\Lambda H} = 0.$$
(36)

The above equation holds the key to unlocking a frequency-stable MFIE. The proof of property (36) is provided in

Appendix A. The term $\mathbb{P}^{\Sigma H}OP^{\Lambda H}$ can now be studied. To this end, note that

$$\alpha^2\mathbb{P}^{\Sigma H}OP^{\Lambda H} =$$
$$= \mathbb{P}^{\Sigma H}\left(\frac{G^{\mathrm{T}}}{2} - K_0\right)\left(G^{\mathrm{T}}\right)^{-1}\left(\frac{G^{\mathrm{T}}}{2} + K_0\right)P^{\Lambda H}$$
$$+\mathbb{P}^{\Sigma H}\left(\frac{G^{\mathrm{T}}}{2} - K_0\right)\left(G^{\mathrm{T}}\right)^{-1}\left(K_k'\right)P^{\Lambda H}$$
$$-\mathbb{P}^{\Sigma H}\left(K_{-jk}'\right)\left(G^{\mathrm{T}}\right)^{-1}\left(\frac{G^{\mathrm{T}}}{2} + K_0\right)P^{\Lambda H} \quad (37)$$
$$-\mathbb{P}^{\Sigma H}\left(K_{-jk}'\right)\left(G^{\mathrm{T}}\right)^{-1}\left(K_k'\right)P^{\Lambda H}$$
$$= 0 + \mathcal{O}(k^2) + \mathcal{O}(k^2) - \mathcal{O}(k^4),$$

which completes the low-frequency analysis of the overall operator

$$O = \mathbb{P}^{\Lambda}OP^{\Sigma} + \mathbb{P}^{\Lambda}OP^{\Lambda H} + \mathbb{P}^{\Sigma H}OP^{\Sigma} + \mathbb{P}^{\Sigma H}OP^{\Lambda H}$$
$$= \mathcal{O}(\alpha^2) + \mathcal{O}(1) + \mathcal{O}(1) + \mathcal{O}\left(\frac{k^2}{\alpha^2}\right).$$
(38)

To choose α we need to consider the physical scaling of the solenoidal and non-solenoidal parts of the current in addition to the conditioning constraint imposed by (38); for a plane wave excitation [6]

$$P^{\Lambda H}j = \mathcal{O}(1),$$
(39)
$$P^{\Sigma}j = \mathcal{O}(k).$$
(40)

These scaling laws reveal that for a standard formulation, a severe loss of significant digits is expected due to the fact that the non-solenoidal component of the current (which scales as $\mathcal{O}(k)$) will disappear when stored alongside the solenoidal component (which scales as $\mathcal{O}(1)$). Instead, for the regularized formulation proposed here, the equation is solved for $i = M^{-1}j$, which scales as

$$P^{\Lambda H}i = \mathcal{O}(\alpha),$$
(41)
$$P^{\Sigma}i = \mathcal{O}(k/\alpha).$$
(42)

It is now evident that by setting $\alpha = \sqrt{k}$, the above scaling behaviors become

$$P^{\Lambda H}i = \mathcal{O}(\sqrt{k}),$$
(43)
$$P^{\Sigma}i = \mathcal{O}(\sqrt{k}),$$
(44)

eliminating the low frequency loss of significance and, at the same time, stabilizing the matrix at low frequencies. The latter is seen upon inserting the new scalings into (38):

$$O = \mathcal{O}(\alpha^2) + \mathcal{O}(1) + \mathcal{O}(1) + \mathcal{O}\left(\frac{k^2}{\alpha^2}\right)$$
$$= \mathcal{O}(k) + \mathcal{O}(1) + \mathcal{O}(1) + \mathcal{O}(k).$$
(45)

The deficiency of the MFIE in the static regime also is solved by the scheme proposed here. In fact, using (38) when $k = 0$ we obtain

$$OP^{\Lambda H} = \mathbb{P}^{\Lambda}OP^{\Lambda H},$$
(46)

which proves the existence of an exact matrix null-space in statics of dimension exactly equal to that of the harmonic subspace.

Formulation	# of Add.	# of Mul.
Mixed MFIE	1	1
New Calderón-like MFIE	7	9
New Calderón-like MFIE at Low Frequency	12	18

This Calderón-like MFIE and its discretization remain compatible with fast solvers and can reach an asymptotic $\mathcal{O}(n\log(n))$ complexity after acceleration with an appropriate fast solver. The computational cost of the new formulation can be compared to that of the mixed MFIE by considering the number of matrix additions and multiplications involved in their respective computations (Table I). However, the cost of the Calderón-like formulation should be studied both in the high and low frequency scenarios to account for the additional cost induced by the explicit cancellation of (36); depending on the type of excitation, explicit cancellations in the right hand side (RHS) of the equation may also require additional matrix operations. The higher overhead of the new formulation at low frequencies is offset by the fact that it is the only magnetic formulation capable of yielding accurate results in this regime and hence a comparison with the mixed MFIE is not appropriate.

Summarizing, the proposed MFIE resolves the three main shortcomings of prior MFIE formulations and can be linearly combined with the EFIE using projectors.

IV. A NEW CFIE

The theoretical developments of the previous sections resulted in a magnetic field operator that can be stably discretized for arbitrarily low frequencies using standard integration rules. The electric counterpart of this operator was obtained in [38]. We will now combine these two operators, first proving the resonance-free property of their continuous combination at high frequencies, and then showing their compatibility at arbitrarily low frequencies.

Standard Calderón CFIE equations use a localization strategy for the EFIE component to obtain a resonance-free equation [22], [23], [55]. Here, we follow the Yukawa-Calderón approach in [22]. When the Yukawa-Calderón EFIE is linearly combined with the new magnetic operator defined in Section III, the following Yukawa-Calderón CFIE is obtained:

$$\left(\eta^2 \left(\frac{\mathcal{I}}{2} - \mathcal{K}_{-\mathrm{j}k} \right) \left(\frac{\mathcal{I}}{2} + \mathcal{K}_k \right) + \mathcal{T}_{-\mathrm{j}k} \mathcal{T}_k \right) (\boldsymbol{j}) =$$
$$\eta^2 \left(\frac{\mathcal{I}}{2} - \mathcal{K}_{-\mathrm{j}k} \right) (\hat{\boldsymbol{n}} \times \boldsymbol{H}^i) + \mathcal{T}_{-\mathrm{j}k} (\hat{\boldsymbol{n}} \times \boldsymbol{E}^i) . \quad (47)$$

To demonstrate that this equation represents a valid Calderón CFIE, i.e. is free from internal resonances, we prove in Appendix B that the operator

$$\left(\eta^2 \left(\frac{\mathcal{I}}{2} - \mathcal{K}_{-\mathrm{j}k} \right) \left(\frac{\mathcal{I}}{2} + \mathcal{K}_k \right) + \mathcal{T}_{-\mathrm{j}k} \mathcal{T}_k \right) \quad (48)$$

can be inverted for any k.

The discretization of the proposed Yukawa-Calderón CFIE follows directly from that of the new MFIE in Section III and that of the EFIE in [38]:

$$\eta^2 \mathbb{M}^{\mathrm{T}} \left(\frac{\boldsymbol{G}^{\mathrm{T}}}{2} - \boldsymbol{K}_{-\mathrm{j}k} \right) (\boldsymbol{G}^{\mathrm{T}})^{-1} \left(\frac{\boldsymbol{G}^{\mathrm{T}}}{2} + \boldsymbol{K}_k \right) \boldsymbol{M} \boldsymbol{i}$$
$$+ \mathbb{M}^{\mathrm{T}} \mathbb{T} \mathbb{M} (\boldsymbol{G})^{-1} \boldsymbol{M}^{\mathrm{T}} \boldsymbol{T} \boldsymbol{M} \boldsymbol{i}$$
$$= \eta^2 \mathbb{M}^{\mathrm{T}} \left(\frac{\boldsymbol{G}^{\mathrm{T}}}{2} - \boldsymbol{K}_{-\mathrm{j}k} \right) (\boldsymbol{G}^{\mathrm{T}})^{-1} \boldsymbol{v}_h$$
$$+ \mathbb{M}^{\mathrm{T}} \mathbb{T} \mathbb{M} (\boldsymbol{G})^{-1} \boldsymbol{M}^{\mathrm{T}} \boldsymbol{v}_e . \quad (49)$$

Here $\alpha = 1$ and $\alpha = \sqrt{k}$ in the high and low frequency regime, respectively; the low frequency regime is characterized by a wavelength smaller than the diameter of the structure. We next study this last regime in more detail.

The appropriate scaling law in the low frequency regime follows from the results of the previous section:

$$\eta^2 \mathbb{M}^{\mathrm{T}} \left(\frac{\boldsymbol{G}^{\mathrm{T}}}{2} - \boldsymbol{K}_{-\mathrm{j}k} \right) (\boldsymbol{G}^{\mathrm{T}})^{-1} \left(\frac{\boldsymbol{G}^{\mathrm{T}}}{2} + \boldsymbol{K}_k \right) \boldsymbol{M} \boldsymbol{i}$$
$$+ \mathbb{M}^{\mathrm{T}} \mathbb{T} \mathbb{M} (\boldsymbol{G})^{-1} \boldsymbol{M}^{\mathrm{T}} \boldsymbol{T} \boldsymbol{M} \boldsymbol{i}$$
$$= - \mathrm{j} \left(\mathbb{P}^{\Sigma H} \mathbb{T}_s \mathbb{P}^{\Sigma H} \right) \boldsymbol{G}^{-1} \boldsymbol{T}_{\mathrm{h}} + \mathrm{j} \mathbb{T}_h \boldsymbol{G}^{-1} \left(\boldsymbol{P}^{\Lambda H} \boldsymbol{T}_s \boldsymbol{P}^{\Lambda H} \right) +$$
$$\mathrm{j} \left(\mathbb{P}^{\Sigma H} \mathbb{T}_s \mathbb{P}^{\Sigma H} \right) \boldsymbol{G}^{-1} \left(\boldsymbol{P}^{\Lambda H} \boldsymbol{T}_s \boldsymbol{P}^{\Lambda H} \right) +$$
$$\eta^2 \mathbb{P}^{\Sigma H} \left(\frac{\boldsymbol{G}^{\mathrm{T}}}{2} - \boldsymbol{K}_0 \right) (\boldsymbol{G}^{\mathrm{T}})^{-1} \left(\frac{\boldsymbol{G}^{\mathrm{T}}}{2} + \boldsymbol{K}_0 \right) \mathrm{j} \boldsymbol{P}^{\Sigma} +$$
$$\eta^2 \mathrm{j} \mathbb{P}^{\Lambda} \left(\frac{\boldsymbol{G}^{\mathrm{T}}}{2} - \boldsymbol{K}_0 \right) (\boldsymbol{G}^{\mathrm{T}})^{-1} \left(\frac{\boldsymbol{G}^{\mathrm{T}}}{2} + \boldsymbol{K}_0 \right) \boldsymbol{P}^{\Lambda H} +$$
$$O(k)$$
$$= \mathcal{O}(1) + \mathcal{O}(1) + \mathcal{O}(1) + \mathcal{O}(1) + \mathcal{O}(1) + \mathcal{O}(k) . \quad (50)$$

Combining this result with the corresponding right hand side scalings (43) and (44) proves the overall low-frequency stability of new CFIE.

Similar to the newly introduced MFIE, the new CFIE formulation can be accelerated with an appropriate fast solvers to attain $\mathcal{O}(n\log(n))$ complexity. The computational costs detailed in Table I can be extended to this new combined field formulation by adding the costs of the Calderón EFIE.

V. NUMERICAL RESULTS

This section presents numerical results that validate the above properties of the proposed MFIE and CFIE.

The first set of tests involve a PEC sphere of radius $1\,\mathrm{m}$. Figure 2 shows the scattered far field at $f = 200\,\mathrm{MHz}$ obtained using the new MFIE and CFIE as well as other established formulations (standard EFIE, EFIE with projectors, Calderón EFIE with projectors, Mixed MFIE, CFIE). For this high frequency simulation all formulations deliver accurate results, thereby validating our implementations. A first difference in performance between our new formulations and their standard counterparts is noted when lowering the frequency. Figure 3 shows data similar to Figure 2 but for $f = 1 \times 10^{-40}\,\mathrm{Hz}$. It is clear that accuracy breakdowns occur for the non-projected methods, i.e. the mixed MFIE, the EFIE, and the CFIE (for the latter two the lack of accuracy also is due to conditioning problems). On the other hand, all projected
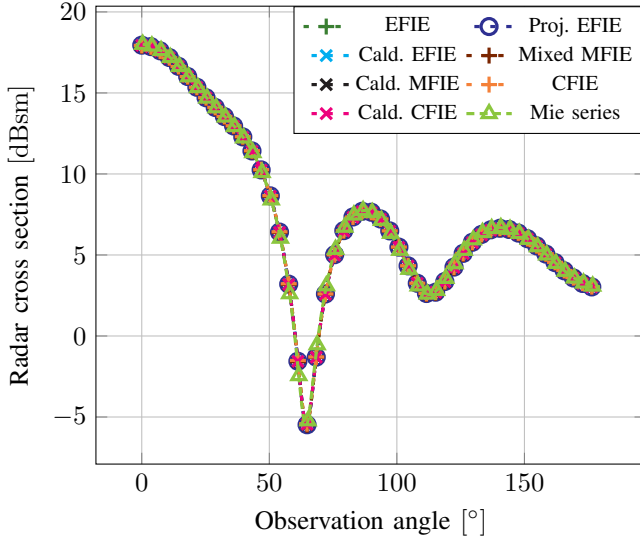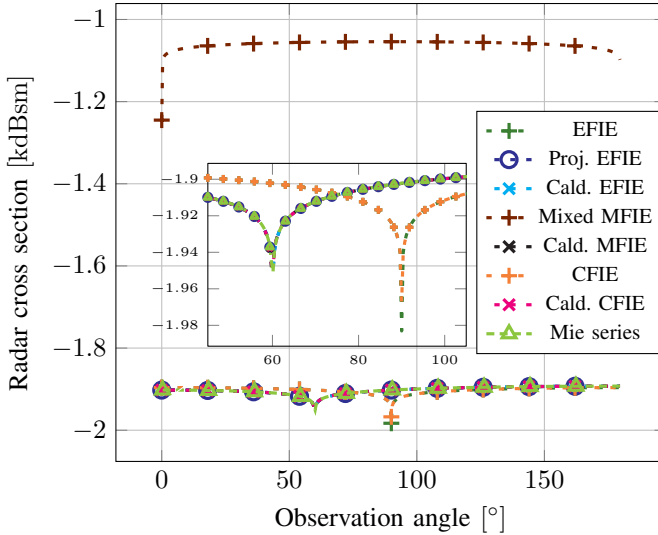
Figure 2. Comparison of the far fields scattered by a PEC sphere of radius 1 m, discretized with an average edge length of 0.15 m, and excited by a 200 MHz plane wave with amplitude of $1\,\text{V m}^{-1}$.
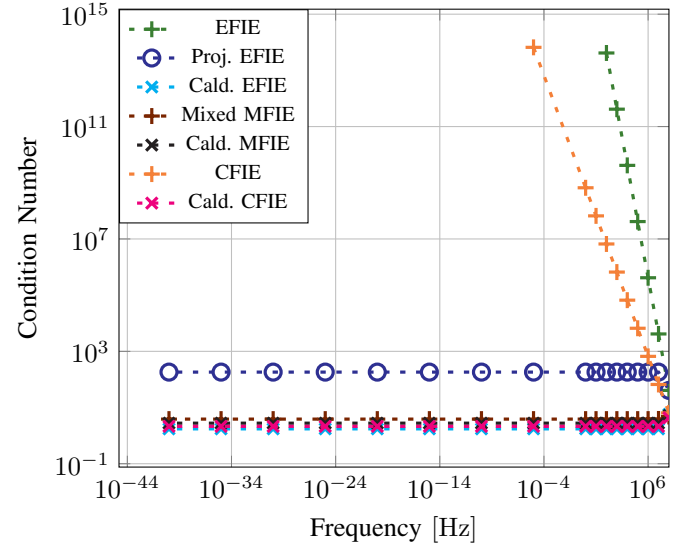

Figure 4. Low frequency behavior of the conditioning of the different formulations on a PEC sphere of radius 1 m. Because of numerical limitations in the computation of very high condition numbers ($> 1 \times 10^{16}$) some points have been left out.

Figure 3. Comparison of the far fields scattered by a PEC sphere of radius 1 m, discretized with an average edge length of 0.15 m, and excited by a 1×10^{-40} Hz plane wave with amplitude of $1\,\text{V m}^{-1}$. The inset is provided for improve the readability of the behavior of the different formulations.
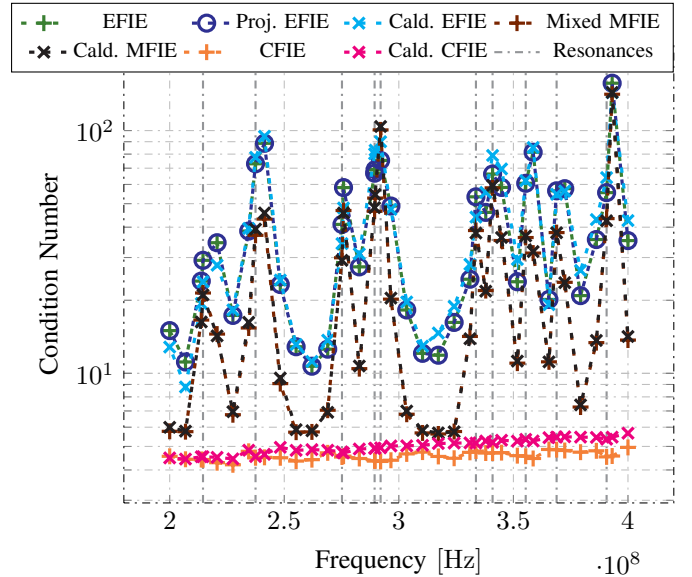

Figure 5. High frequency behavior of the conditioning of the different formulations on a PEC sphere of radius 1 m sphere illustrating the spurious resonances occurring in non-combined formulations. The average edge size of the discretized sphere has been kept at one-fifth of the wavelength for every simulation.

formulations, including the two new ones, deliver accurate results for arbitrarily low frequencies.

The low frequency stability of the new Calderón MFIE is further demonstrated in Figure 4, which illustrates the conditioning of the different formulations for low frequencies. It is clear that the new MFIE remains as well-conditioned as its standard counterpart. The Calderón CFIE is also low-frequency stable, unlike the standard CFIE, which exhibits a severe ill-conditioning caused by its EFIE contribution.

Figure 5 shows that, despite its regularized low frequency behavior, the Calderón MFIE is prone to spurious resonances causing it to become periodically ill-conditioned. This issue is shared by all non-combined formulations and can be overcome by combined field strategies. It is clear from the figure that both the new Calderón CFIE and its standard counterpart exhibit resonance-free behavior.

The last key property to be illustrated is the refinement stability of the proposed formulations. This property was verified by studying the dependence of the condition number of the different formulations applied to a unit radius sphere with increasing discretization density (Figure 6). These results confirm that the second kind nature of our new formulations
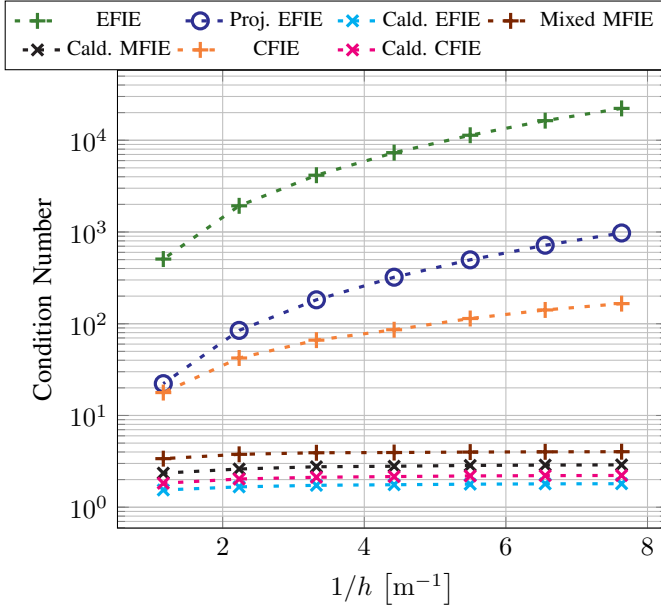
Figure 6. Dense discretization behavior of the conditioning of the different formulations on a PEC sphere of radius $1\,\mathrm{m}$. The non-resonant frequency has been kept constant for all simulations and corresponds to 5 unknowns per wavelength discretization for the least refined point.

Figure 7. Comparison of the far fields scattered by a PEC square torus of inner radius $0.5\,\mathrm{m}$ and tube radius $0.25\,\mathrm{m}$, discretized with an average edge length of $0.15\,\mathrm{m}$, and excited by a $200\,\mathrm{MHz}$ plane wave with amplitude of $1\,\mathrm{V\,m^{-1}}$.

Figure 8. Comparison of the far fields scattered by a PEC square torus of inner radius $0.5\,\mathrm{m}$ and tube radius $0.25\,\mathrm{m}$, discretized with an average edge length of $0.15\,\mathrm{m}$, and excited by a $1 \times 10^{-40}\,\mathrm{Hz}$ plane wave with amplitude of $1\,\mathrm{V\,m^{-1}}$.

renders them immune to the dense discretization breakdown.

In summary, the above results show that the new Calderón MFIE yields correct results for arbitrarily low frequencies, and is well conditioned for both low frequencies and dense discretizations. Additionally, when combining this MFIE with the projector Calderón EFIE, a new Calderón CFIE is obtained that is low frequency stable, immune to dense discretization breakdown, and free from non-physical resonances.

To ensure that the properties illustrated so far still persist for multiply connected structures, many of the previous analyses were repeated for a square torus (obtained by connecting the ends of a cylinder of square cross-section). The correctness of the formulation has been verified by studying the far field scattered by the torus at high and very low frequencies, respectively (Figures 7 and 8). Since no analytic solution is readily available for the square torus, the solution of the Calderón EFIE was used as a reference and particular care was taken to avoid frequencies corresponding to an internal resonance. While the results are similar to those of the sphere, the reader should be aware that, because of its toroidal and poloidal null-spaces, the Calderón MFIE required the usage of a pseudo-inversion to obtain current solutions at very low frequencies.

The low frequency stability of the Calderón MFIE and Calderón CFIE on the toroidal structure are demonstrated in Figure 9, while their resonance-free behaviors are illustrated in Figure 10. Finally, the resilience of both formulations to dense discretization breakdown is illustrated in Figure 11, which presents the condition number of the discretized integral operators with increasing discretization.

One of the key advantages of the new Calderón MFIE scheme is that it does not require extremely accurate numerical
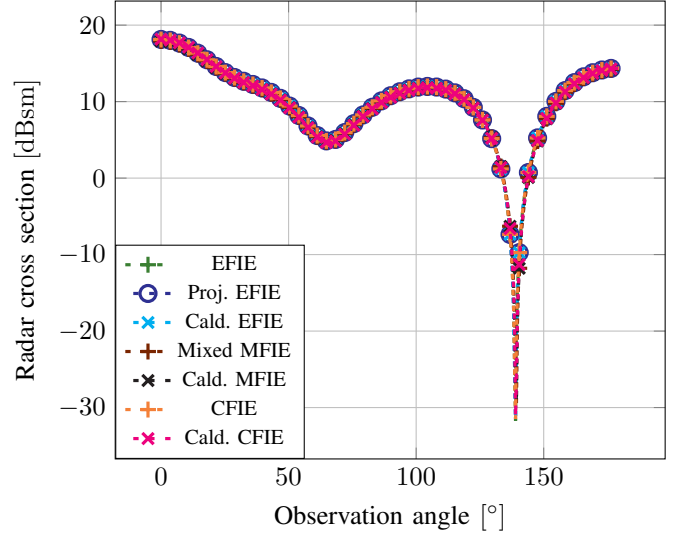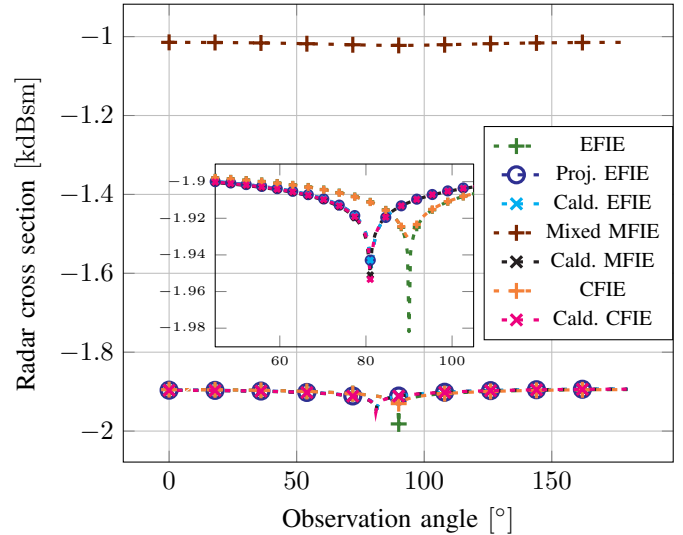
integration rules because it allows explicit cancellation of near-zero terms. In other words, when implementing (33), the matrix product should be expanded and (36) must be explicitly set to **0** to obtain accurate results even with low-order numerical integration rules. The slow convergence of the standard numerical integration schemes can be seen in Figure 12, in which the ratio of the norm of the term in (36) to the norm of the full operator with increasing number of integration points is presented. While this ratio does decrease with the number of Gaussian quadrature points, it does so very slowly and remains far from a machine-precision zero. The effect of these numerical inaccuracies is evident when comparing the singular
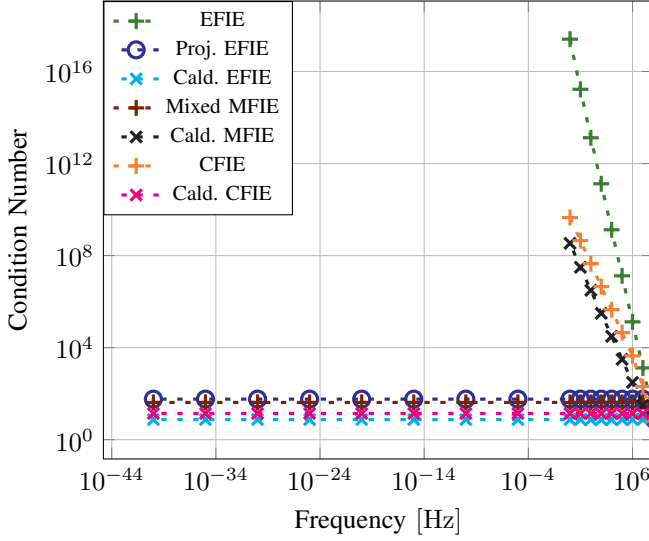
Figure 9. Low frequency behavior of the conditioning of the different formulations on a PEC square torus with an inner radius of 0.5 m, a tube radius of 0.25 m and meshed with an average edge length of 0.6 m.
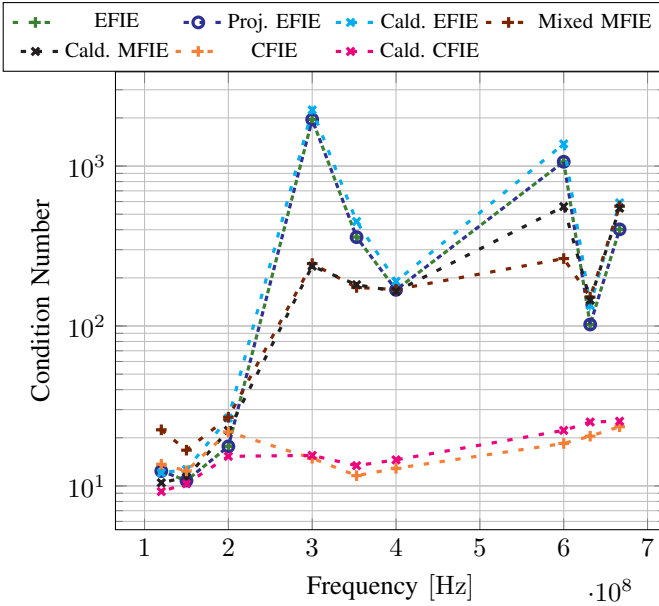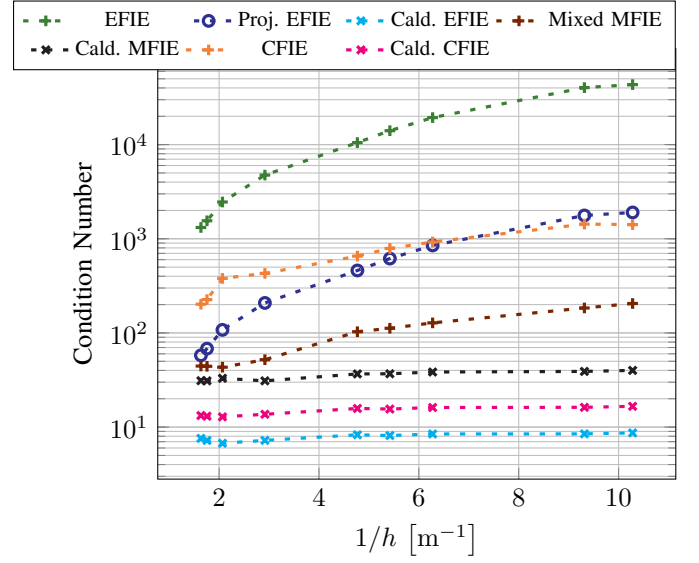

Figure 11. Dense discretization behavior of the conditioning of the different formulations on a PEC square torus of inner radius of 0.5 m and tube radius of 0.25 m. The non-resonant frequency is kept constant and corresponds to a 5 unknowns per wavelength discretization for the least refined point.

Figure 10. High frequency behavior of the conditioning of the different formulations on a PEC square torus of inner radius of 0.5 m and tube radius of 0.25 m, illustrating the resonances of non-combined formulations. The average edge size of the discretization is kept at one-fifth of the wavelength.
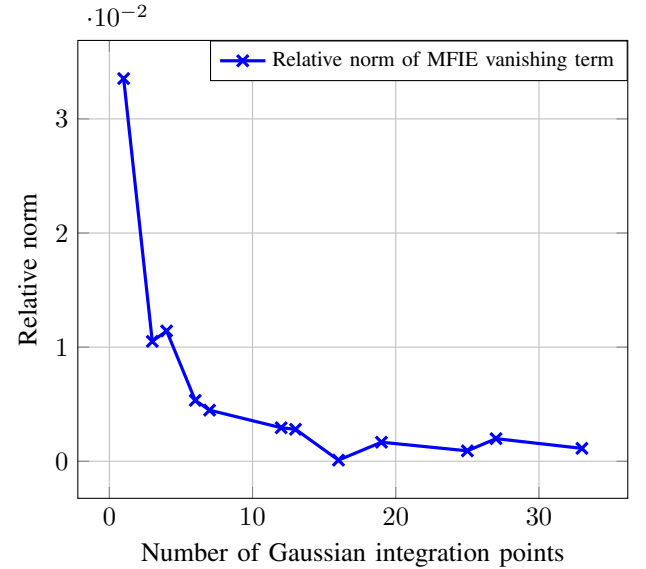

Figure 12. Decay of the relative (with regards to the full operator) norm of cancelled out term (51) of the Calderón CFIE as a function of the number of Gaussian integration points. These results correspond to a square torus of inner radius 0.5 m and tube radius 0.25 m simulated at 1×10^{-10} Hz.

value decompositions of the Mixed MFIE and of the new Calderón MFIE in Figure 13. It is clear that the null singular values corresponding to the toroidal and poloidal subspaces of the square torus immediately reach the machine precision zero in the case of the Calderón MFIE, while for the Mixed MFIE they require an unreasonably complex integration rules to even remotely resemble a nullspace.

Finally, to demonstrate that our schemes can be readily applied to more complex problems we studied the low frequency conditioning of our operators (Figure 15) for the complex,

multiply connected geometry in Figure 14.

VI. CONCLUSION

This paper presented a new Calderón-like MFIE that can be stably and effectively discretized using quasi-Helmholtz projectors. When linearly combined with a quasi-Helmholtz projector-based Calderón EFIE, a new CFIE that is immune from all drawbacks that plague the majority of existing formulations is obtained. In fact, the proposed CFIE remains well-conditioned both at low frequencies and for dense discretiza-
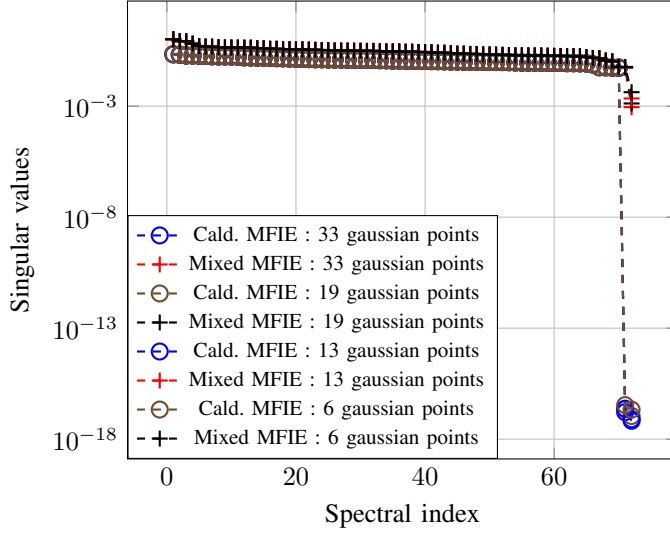
Figure 13. Accuracy of the toroidal and poloidal nullspaces obtained by the Calderón and Mixed MFIE as a function of the number of Gaussian integration points. The results correspond to a square torus of inner radius $0.5\,\mathrm{m}$ and tube radius $0.25\,\mathrm{m}$ simulated at $1 \times 10^{-10}\,\mathrm{Hz}$.

Figure 15. Low frequency behavior of the conditioning of the different formulations on the structure illustrated in Figure 14. Because of numerical limitations in the computation of very high condition numbers ($> 1 \times 10^{16}$) some points have been left out.
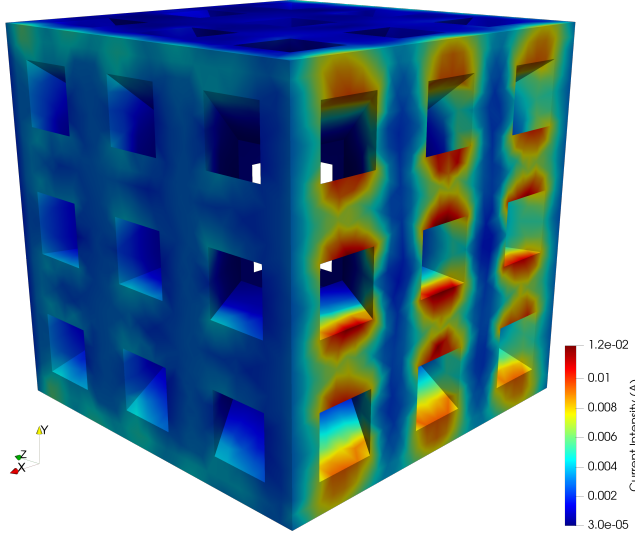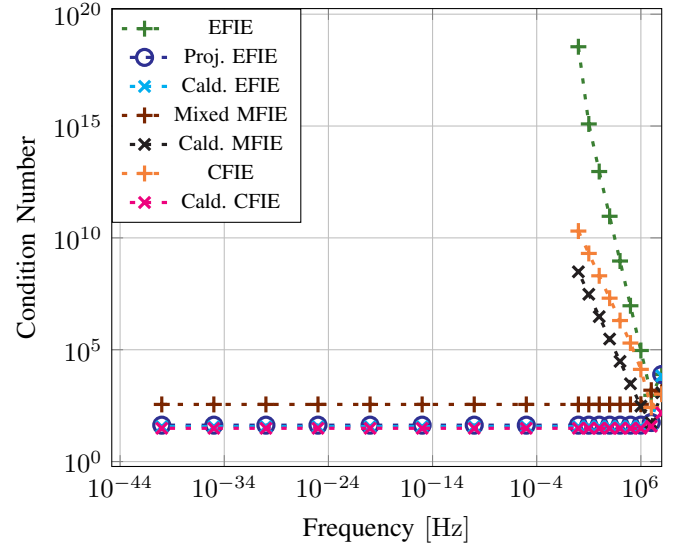

Figure 14. Complex multiply-connected cube-like geometry with $9\,\mathrm{m}$ side-length and discretized with an average edge length of $0.35\,\mathrm{m}$. The values represented on the geometry correspond to the intensity of the current induced on the PEC structure by a plane wave oscillating at $8.5 \times 10^7\,\mathrm{Hz}$ and directed along the $\hat{z}$ axis.

tion densities, allows for an accurate solution at extremely low frequencies without requiring special numerical quadrature methods, does not require the detection of global loops when applied to multiply connected geometries, and is provably free from internal resonances. Numerical results confirm the theoretically predicted properties of the proposed equations.

Appendix A
Proof of the Fundamental Matrix Relationship (36)

To prove the validity of (36), i.e.

$$\mathbb{P}^{\Sigma H}\left(\frac{\boldsymbol{G}^{\mathrm{T}}}{2} - \boldsymbol{K}_0\right)\left(\boldsymbol{G}^{\mathrm{T}}\right)^{-1}\left(\frac{\boldsymbol{G}^{\mathrm{T}}}{2} + \boldsymbol{K}_0\right)\boldsymbol{P}^{\Lambda H} = \boldsymbol{0}, \quad (51)$$

we introduce $\boldsymbol{P}^{\mathrm{Pol}}$, $\boldsymbol{P}^{\mathrm{Tor}}$, $\mathbb{P}^{\mathrm{Pol}}$, $\mathbb{P}^{\mathrm{Tor}}$, the orthogonal projectors into the right and left null-spaces of the internal and external MFIE operators, i.e.

$$\left(\frac{\boldsymbol{G}^{\mathrm{T}}}{2} + \boldsymbol{K}_0\right)\boldsymbol{P}^{\mathrm{Pol}} = \boldsymbol{0}, \quad (52)$$

$$\left(\frac{\boldsymbol{G}^{\mathrm{T}}}{2} - \boldsymbol{K}_0\right)\boldsymbol{P}^{\mathrm{Tor}} = \boldsymbol{0}, \quad (53)$$

$$\mathbb{P}^{\mathrm{Pol}}\left(\frac{\boldsymbol{G}^{\mathrm{T}}}{2} - \boldsymbol{K}_0\right) = \boldsymbol{0}, \quad (54)$$

$$\mathbb{P}^{\mathrm{Tor}}\left(\frac{\boldsymbol{G}^{\mathrm{T}}}{2} + \boldsymbol{K}_0\right) = \boldsymbol{0}. \quad (55)$$

Note that

$$\left(\frac{\boldsymbol{G}^{\mathrm{T}}}{2} + \boldsymbol{K}_0\right)\boldsymbol{P}^{\mathrm{Tor}} = \boldsymbol{G}^{\mathrm{T}}\boldsymbol{P}^{\mathrm{Tor}}, \quad (56)$$

$$\left(\frac{\boldsymbol{G}^{\mathrm{T}}}{2} - \boldsymbol{K}_0\right)\boldsymbol{P}^{\mathrm{Pol}} = \boldsymbol{G}^{\mathrm{T}}\boldsymbol{P}^{\mathrm{Pol}}, \quad (57)$$

$$\mathbb{P}^{\mathrm{Tor}}\left(\frac{\boldsymbol{G}^{\mathrm{T}}}{2} - \boldsymbol{K}_0\right) = \mathbb{P}^{\mathrm{Tor}}\boldsymbol{G}^{\mathrm{T}}, \quad (58)$$

$$\mathbb{P}^{\mathrm{Pol}}\left(\frac{\boldsymbol{G}^{\mathrm{T}}}{2} + \boldsymbol{K}_0\right) = \mathbb{P}^{\mathrm{Pol}}\boldsymbol{G}^{\mathrm{T}}. \quad (59)$$

We next define

$$\mathbb{Q}^{\Lambda} = \boldsymbol{P}^{\Lambda H} - \boldsymbol{P}^{\mathrm{Pol}} - \boldsymbol{P}^{\mathrm{Tor}}, \quad (60)$$

which clearly satisfies

$$\mathbb{P}^{\Lambda}\mathbb{Q}^{\Lambda} = \mathbb{Q}^{\Lambda}, \quad (61)$$

since the union of the right null spaces of the internal and external MFIE operators contains all the non-trivial cycles of the structure [48]. In addition, the operator

$$Q^{\Sigma} = \mathbb{P}^{\Sigma H} - \mathbb{P}^{\text{Pol}} - \mathbb{P}^{\text{Tor}}, \tag{62}$$

satisfies

$$P^{\Sigma} Q^{\Sigma} = Q^{\Sigma}. \tag{63}$$

It follows that

$$
\begin{aligned}
&\left(\frac{G^{\text{T}}}{2} - K_0\right)\left(G^{\text{T}}\right)^{-1}\left(\frac{G^{\text{T}}}{2} + K_0\right) P^{\Lambda H} \\
&= \left(\frac{G^{\text{T}}}{2} - K_0\right)\left(G^{\text{T}}\right)^{-1}\left(\frac{G^{\text{T}}}{2} + K_0\right)\left(\mathbb{Q}^{\Lambda} + P^{\text{Pol}} + P^{\text{Tor}}\right) \\
&= \left(\frac{G^{\text{T}}}{2} - K_0\right)\left(G^{\text{T}}\right)^{-1}\left(\frac{G^{\text{T}}}{2} + K_0\right) \mathbb{Q}^{\Lambda} \\
&\quad + \left(\frac{G^{\text{T}}}{2} - K_0\right)\left(G^{\text{T}}\right)^{-1}\left(\frac{G^{\text{T}}}{2} + K_0\right) P^{\text{Tor}} \\
&= \left(\frac{G^{\text{T}}}{2} - K_0\right)\left(G^{\text{T}}\right)^{-1}\left(\frac{G^{\text{T}}}{2} + K_0\right) \mathbb{Q}^{\Lambda} \\
&\quad + \left(\frac{G^{\text{T}}}{2} - K_0\right) P^{\text{Tor}} \\
&= \left(\frac{G^{\text{T}}}{2} - K_0\right)\left(G^{\text{T}}\right)^{-1}\left(\frac{G^{\text{T}}}{2} + K_0\right) \mathbb{Q}^{\Lambda},
\end{aligned} \tag{64}
$$

and similarly that

$$
\begin{aligned}
&\mathbb{P}^{\Sigma H}\left(\frac{G^{\text{T}}}{2} - K_0\right)\left(G^{\text{T}}\right)^{-1}\left(\frac{G^{\text{T}}}{2} + K_0\right) \\
&= Q^{\Sigma}\left(\frac{G^{\text{T}}}{2} - K_0\right)\left(G^{\text{T}}\right)^{-1}\left(\frac{G^{\text{T}}}{2} + K_0\right).
\end{aligned} \tag{65}
$$

Combining the above equations it follows that

$$
\begin{aligned}
&\mathbb{P}^{\Sigma H}\left(\frac{G^{\text{T}}}{2} - K_0\right)\left(G^{\text{T}}\right)^{-1}\left(\frac{G^{\text{T}}}{2} + K_0\right) P^{\Lambda H} \\
&= Q^{\Sigma}\left(\frac{G^{\text{T}}}{2} - K_0\right)\left(G^{\text{T}}\right)^{-1}\left(\frac{G^{\text{T}}}{2} + K_0\right) \mathbb{Q}^{\Lambda}.
\end{aligned} \tag{66}
$$

In the above expression we now insert the identity matrices $\left(P^{\Lambda H} + P^{\Sigma}\right)$ and $\left(\mathbb{P}^{\Sigma H} + \mathbb{P}^{\Lambda}\right)$ obtaining

$$
\begin{aligned}
(66) &= Q^{\Sigma}\left(\frac{G^{\text{T}}}{2} - K_0\right)\left(P^{\Lambda H} + P^{\Sigma}\right)\left(G^{\text{T}}\right)^{-1} \\
&\quad \left(\mathbb{P}^{\Sigma H} + \mathbb{P}^{\Lambda}\right)\left(\frac{G^{\text{T}}}{2} + K_0\right) \mathbb{Q}^{\Lambda}.
\end{aligned} \tag{67}
$$

Given that

$$Q^{\Sigma}\left(\frac{G^{\text{T}}}{2} - K_0\right) P^{\Lambda H} = Q^{\Sigma} P^{\Sigma}\left(\frac{G^{\text{T}}}{2} - K_0\right) P^{\Lambda H} = 0 \tag{68}$$

and that

$$\mathbb{P}^{\Sigma H}\left(\frac{G^{\text{T}}}{2} + K_0\right) \mathbb{Q}^{\Lambda} = \mathbb{P}^{\Sigma H}\left(\frac{G^{\text{T}}}{2} + K_0\right) \mathbb{P}^{\Lambda} \mathbb{Q}^{\Lambda} = 0 \tag{69}$$

and considering the property

$$P^{\Sigma}\left(G^{\text{T}}\right)^{-1} \mathbb{P}^{\Lambda} = 0, \tag{70}$$

it follows that

$$
\begin{aligned}
(66) &= P^{\Sigma}\left(\frac{G^{\text{T}}}{2} - K_0\right) P^{\Sigma}\left(G^{\text{T}}\right)^{-1} \mathbb{P}^{\Lambda}\left(\frac{G^{\text{T}}}{2} + K_0\right) \mathbb{P}^{\Lambda} \\
&= 0,
\end{aligned} \tag{71}
$$

which completes the proof.

APPENDIX B
RESONANCE-FREE PROOF FOR THE NEW CALDERÓN CFIE OPERATOR

Since the operator $\left(\frac{\mathcal{I}}{2} - \mathcal{K}_{-jk}\right)$ always admits an inverse, the invertibility of (48) is equivalent to the invertibility of

$$\left(\frac{\mathcal{I}}{2} + \mathcal{K}_k\right) + \left(\frac{\mathcal{I}}{2} - \mathcal{K}_{-jk}\right)^{-1} \mathcal{T}_{-jk} \mathcal{T}_k. \tag{72}$$

Given the anti-commutation property

$$\mathcal{T}^{-1}\mathcal{K} + \mathcal{K}\mathcal{T}^{-1} = 0, \tag{73}$$

which follows directly from the second Calderón identity $\mathcal{T}^{-1}\mathcal{K} = \mathcal{T}^{-1}\mathcal{K}\mathcal{T}\mathcal{T}^{-1} = -\mathcal{T}^{-1}\mathcal{T}\mathcal{K}\mathcal{T}^{-1} = -\mathcal{K}\mathcal{T}^{-1}$, and defining

$$\mathcal{A} = \left(\frac{\mathcal{I}}{2} - \mathcal{K}_{-jk}\right)^{-1} \mathcal{T}_{-jk}, \tag{74}$$

it follows that

$$
\begin{aligned}
(\hat{n} \times \mathcal{A})^{\text{T}} &= \left(\hat{n} \times \left(\frac{\mathcal{I}}{2} - \mathcal{K}_{-jk}\right)^{-1} \mathcal{T}_{-jk}\right)^{\text{T}} \\
&= \left(\hat{n} \times \left(\mathcal{T}_{-jk}^{-1}\left(\frac{\mathcal{I}}{2} - \mathcal{K}_{-jk}\right)\right)^{-1}\right)^{\text{T}} \\
&= \left(\hat{n} \times \left(\left(\frac{\mathcal{I}}{2} + \mathcal{K}_{-jk}\right) \mathcal{T}_{-jk}^{-1}\right)^{-1}\right)^{\text{T}} \\
&= \left(\hat{n} \times \mathcal{T}_{-jk}\left(\frac{\mathcal{I}}{2} + \mathcal{K}_{-jk}\right)^{-1}\right)^{\text{T}} \\
&= \left(\left(\frac{\mathcal{I}}{2} + \mathcal{K}_{-jk}\right)^{-1}\right)^{\text{T}} \hat{n} \times \mathcal{T}_{-jk} \\
&= -\hat{n} \times \left(\frac{\mathcal{I}}{2} - \mathcal{K}_{-jk}\right)^{-1} \hat{n} \times \hat{n} \times \mathcal{T}_{-jk} \\
&= \hat{n} \times \left(\frac{\mathcal{I}}{2} - \mathcal{K}_{-jk}\right)^{-1} \mathcal{T}_{-jk} \\
&= \hat{n} \times \mathcal{A}.
\end{aligned} \tag{75}
$$

Given this result and the fact that

$$\hat{n} \times \mathcal{A} = \hat{n} \times \left(\frac{\mathcal{I}}{2} - \mathcal{K}_{-jk}\right)^{-1} \mathcal{T}_{-jk} \tag{76}$$

is a real operator, the symmetry implies it being Hermitian, so that

$$x^{\dagger}\left(\hat{n} \times \left(\frac{\mathcal{I}}{2} - \mathcal{K}_{-jk}\right)^{-1} \mathcal{T}_{-jk}\right) x \tag{77}$$

is real and nonzero. By leveraging a straightforward extension of Theorem 3.1 in [56], it follows that

$$\left(\left(\frac{\mathcal{I}}{2} - \mathcal{K}_{-jk}\right)\left(\frac{\mathcal{I}}{2} + \mathcal{K}_k\right) + \mathcal{T}_{-jk}\mathcal{T}_k\right) \tag{78}$$

is always invertible. Otherwise said, the proposed Yukawa-Calderón CFIE is resonance free.

REFERENCES

[1] J. G. Van Bladel, *Electromagnetic Fields*, 2nd ed., ser. IEEE Press Series on Electromagnetic Wave Theory. Piscataway, NJ: IEEE Press, 2007.

[2] J. R. Mautz and R. F. Harrington, "H-Field, E-Field, and Combined Field Solutions for Bodies of Revolution:," Defense Technical Information Center, Fort Belvoir, VA, Tech. Rep., Mar. 1977.

[3] S. Rao, D. Wilton, and A. Glisson, "Electromagnetic scattering by surfaces of arbitrary shape," *IEEE Transactions on Antennas and Propagation*, vol. 30, no. 3, pp. 409–418, May 1982.

[4] K. Cools, F. P. Andriulli, D. De Zutter, and E. Michielssen, "Accurate and Conforming Mixed Discretization of the MFIE," *IEEE Antennas and Wireless Propagation Letters*, vol. 10, pp. 528–531, 2011.

[5] Yunhua Zhang, Tie Jun Cui, Weng Cho Chew, and Jun-Sheng Zhao, "Magnetic field integral equation at very low frequencies," *IEEE Transactions on Antennas and Propagation*, vol. 51, no. 8, pp. 1864–1871, Aug. 2003.

[6] Z.-G. Qian and W. C. Chew, "Enhanced A-EFIE With Perturbation Method," *IEEE Transactions on Antennas and Propagation*, vol. 58, no. 10, pp. 3256–3264, Oct. 2010.

[7] Z. G. Qian and W. C. Chew, "A quantitative study on the low frequency breakdown of EFIE," *Microwave and Optical Technology Letters*, vol. 50, no. 5, pp. 1159–1162, May 2008.

[8] D. Wilton and A. Glisson, "On improving the stability of the electric field integral equation at low frequencies," in *1981 USNC/URSI Spring Meeting Digestt*, Los Angeles, California, June 1981, p. 24.

[9] G. Vecchi, "Loop-star decomposition of basis functions in the discretization of the EFIE," *Antennas and Propagation, IEEE Transactions on*, vol. 47, no. 2, pp. 339–346, 1999.

[10] J.-S. Zhao and W. C. Chew, "Integral equation solution of Maxwell's equations from zero frequency to microwave frequencies," *Antennas and Propagation, IEEE Transactions on*, vol. 48, no. 10, pp. 1635–1645, 2000.

[11] J.-F. Lee, R. Lee, and R. Burkholder, "Loop star basis functions and a robust preconditioner for EFIE scattering problems," *IEEE Transactions on Antennas and Propagation*, vol. 51, no. 8, pp. 1855–1863, Aug. 2003.

[12] T. F. Eibert, "Iterative-solver convergence for loop-star and loop-tree decompositions in method-of-moments solutions of the electric-field integral equation," *Antennas and Propagation Magazine, IEEE*, vol. 46, no. 3, pp. 80–85, 2004.

[13] F. P. Andriulli, A. Tabacco, and G. Vecchi, "Solving the EFIE at Low Frequencies With a Conditioning That Grows Only Logarithmically With the Number of Unknowns," *IEEE Transactions on Antennas and Propagation*, vol. 58, no. 5, pp. 1614–1624, May 2010.

[14] F. P. Andriulli, K. Cools, H. Bagci, F. Olyslager, A. Buffa, S. Christiansen, and E. Michielssen, "A Multiplicative Calderon Preconditioner for the Electric Field Integral Equation," *IEEE Transactions on Antennas and Propagation*, vol. 56, no. 8, pp. 2398–2412, Aug. 2008.

[15] F. P. Andriulli, "Loop-Star and Loop-Tree Decompositions: Analysis and Efficient Algorithms," *IEEE Transactions on Antennas and Propagation*, vol. 60, no. 5, pp. 2347–2356, May 2012.

[16] Z. G. Qian and W. C. Chew, "An augmented electric field integral equation for high-speed interconnect analysis," *Microwave and Optical Technology Letters*, vol. 50, no. 10, pp. 2658–2662, Oct. 2008.

[17] J. Zhu and D. Jiao, "A Rigorous Solution to the Low-Frequency Breakdown in Full-Wave Finite-Element-Based Analysis of General Problems Involving Inhomogeneous Lossless/Lossy Dielectrics and Nonideal Conductors," *IEEE Transactions on Microwave Theory and Techniques*, vol. 59, no. 12, pp. 3294–3306, Dec. 2011.

[18] J. Zhu, S. Omar, and D. Jiao, "Solution of the Electric Field Integral Equation When It Breaks Down," *IEEE Transactions on Antennas and Propagation*, vol. 62, no. 8, pp. 4122–4134, Aug. 2014.

[19] F. Vipiana, G. Vecchi, and P. Pirinoli, "A Multiresolution System of Rao–Wilton–Glisson Functions," *IEEE Transactions on Antennas and Propagation*, vol. 55, no. 3, pp. 924–930, Mar. 2007.

[20] F. P. Andriulli, F. Vipiana, and G. Vecchi, "Hierarchical Bases for Nonhierarchic 3-D Triangular Meshes," *IEEE Transactions on Antennas and Propagation*, vol. 56, no. 8, pp. 2288–2297, Aug. 2008.

[21] R. Chen, J. Ding, D. Z. Ding, Z. H. Fan, and D. Wang, "A Multiresolution Curvilinear Rao–Wilton–Glisson Basis Function for Fast Analysis of Electromagnetic Scattering," *IEEE Transactions on Antennas and Propagation*, vol. 57, no. 10, pp. 3179–3188, Oct. 2009.

[22] H. Contopanagos, B. Dembart, M. Epton, J. Ottusch, V. Rokhlin, J. Visher, and S. Wandzura, "Well-conditioned boundary integral equations for three-dimensional electromagnetic scattering," *IEEE Transactions on Antennas and Propagation*, vol. 50, no. 12, pp. 1824–1830, Dec. 2002.

[23] R. Adams, "Physical and Analytical Properties of a Stabilized Electric Field Integral Equation," *IEEE Transactions on Antennas and Propagation*, vol. 52, no. 2, pp. 362–372, Feb. 2004.

[24] M. Darbas, "Generalized combined field integral equations for the iterative solution of the three-dimensional Maxwell equations," *Applied Mathematics Letters*, vol. 19, no. 8, pp. 834–839, Aug. 2006.

[25] P. Yla-Oijala, S. P. Kiminki, and S. Jarvenpaa, "Calderon Preconditioned Surface Integral Equations for Composite Objects With Junctions," *IEEE Transactions on Antennas and Propagation*, vol. 59, no. 2, pp. 546–554, Feb. 2011.

[26] D. Dobbelaere, D. De Zutter, J. Van Hese, J. Sercu, T. Boonen, and H. Rogier, "A Calderón multiplicative preconditioner for the electromagnetic Poincaré–Steklov operator of a heterogeneous domain with scattering applications," *Journal of Computational Physics*, vol. 303, pp. 355–371, Dec. 2015.

[27] M. Gossye, M. Huynen, D. V. Ginste, D. D. Zutter, and H. Rogier, "A Calderón Preconditioner for High Dielectric Contrast Media," *IEEE Transactions on Antennas and Propagation*, vol. 66, no. 2, pp. 808–818, Feb. 2018.

[28] C. L. Epstein and L. Greengard, "Debye sources and the numerical solution of the time harmonic Maxwell equations," *Communications on Pure and Applied Mathematics*, vol. 63, no. 4, pp. 413–463, 2010.

[29] S. H. Christiansen and J.-C. Nedelec, "A Preconditioner for the Electric Field Integral Equation Based on Calderon Formulas," *SIAM Journal on Numerical Analysis*, vol. 40, no. 3, pp. 1100–1135, Jan. 2002.

[30] M. B. Stephanson and J.-F. Lee, "Preconditioned Electric Field Integral Equation Using Calderon Identities and Dual Loop/Star Basis Functions," *IEEE Transactions on Antennas and Propagation*, vol. 57, no. 4, pp. 1274–1279, Apr. 2009.

[31] Su Yan, Jian-Ming Jin, and Zaiping Nie, "EFIE Analysis of Low-Frequency Problems With Loop-Star Decomposition and Calderón Multiplicative Preconditioner," *IEEE Transactions on Antennas and Propagation*, vol. 58, no. 3, pp. 857–867, Mar. 2010.

[32] W. C. Chew, M. S. Tong, and B. Hu, *Integral Equation Methods for Electromagnetic and Elastic Waves*. Morgan & Claypool Publishers, Jan. 2008, vol. 3.

[33] I. Bogaert, K. Cools, F. P. Andriulli, and H. Bagci, "Low-Frequency Scaling of the Standard and Mixed Magnetic Field and Müller Integral Equations," *IEEE Transactions on Antennas and Propagation*, vol. 62, no. 2, pp. 822–831, Feb. 2014.

[34] F. Vico, M. Ferrando, L. Greengard, and Z. Gimbutas, "The Decoupled Potential Integral Equation for Time-Harmonic Electromagnetic Scattering," *Communications on Pure and Applied Mathematics*, vol. 69, no. 4, pp. 771–812, Apr. 2016.

[35] S. Sun, Y. G. Liu, W. C. Chew, and Z. Ma, "Calderón Multiplicative Preconditioned EFIE With Perturbation Method," *IEEE Transactions on Antennas and Propagation*, vol. 61, no. 1, pp. 247–255, Jan. 2013.

[36] J. Cheng, R. J. Adams, J. C. Young, and M. A. Khayat, "Augmented EFIE With Normally Constrained Magnetic Field and Static Charge Extraction," *IEEE Transactions on Antennas and Propagation*, vol. 63, no. 11, pp. 4952–4963, Nov. 2015.

[37] A. Das and D. Gope, "Modified Separated Potential Integral Equation for Low-Frequency EFIE Conditioning," *IEEE Transactions on Antennas and Propagation*, vol. 64, no. 4, pp. 1394–1403, Apr. 2016.

[38] F. P. Andriulli, K. Cools, I. Bogaert, and E. Michielssen, "On a Well-Conditioned Electric Field Integral Operator for Multiply Connected Geometries," *IEEE Transactions on Antennas and Propagation*, vol. 61, no. 4, pp. 2077–2087, Apr. 2013.

[39] Y. Beghein, K. Cools, and F. P. Andriulli, "A DC Stable and Large-Time Step Well-Balanced TD-EFIE Based on Quasi-Helmholtz Projectors," *IEEE Transactions on Antennas and Propagation*, vol. 63, no. 7, pp. 3087–3097, Jul. 2015.

[40] ——, "A DC-Stable, Well-Balanced, Calderón Preconditioned Time Domain Electric Field Integral Equation," *IEEE Transactions on Antennas and Propagation*, vol. 63, no. 12, pp. 5650–5660, Dec. 2015.

[41] Y. Beghein, R. Mitharwal, K. Cools, and F. P. Andriulli, "Handling the low-frequency breakdown of the PMCHWT integral equation with the quasi-Helmholtz projectors," in *2015 International Conference on Electromagnetics in Advanced Applications (ICEAA)*, Sep. 2015, pp. 1534–1537.

[42] Y. Beghein, K. Cools, and F. P. Andriulli, "A robust and low frequency stable time domain PMCHWT equation," in *2015 International Conference on Electromagnetics in Advanced Applications (ICEAA)*, Sep. 2015, pp. 954–957.

[43] J. Markkanen, "Discrete Helmholtz Decomposition for Electric Current Volume Integral Equation Formulation," *IEEE Transactions on Antennas and Propagation*, vol. 62, no. 12, pp. 6282–6289, Dec. 2014.

[44] W. C. Chew and J. M. Song, "Gedanken Experiments to Understand the Internal Resonance Problems of Electromagnetic Scattering," *Electromagnetics*, vol. 27, no. 8, pp. 457–471, Nov. 2007.

[45] F. P. Andriulli, I. Bogaert, K. Cools, and E. Michielssen, "A magnetic type integral operator which is stable till extremely low frequencies," in *2014 XXXIth URSI General Assembly and Scientific Symposium (URSI GASS)*, Aug. 2014, pp. 1–4.

[46] ——, "A well-conditioned combined field integral equation based on quasi-helmholtz projectors," in *2013 International Conference on Electromagnetics in Advanced Applications (ICEAA)*, Sep. 2013, pp. 644–647.

[47] A. Buffa and S. Christiansen, "A dual finite element complex on the barycentric refinement," *Mathematics of Computation*, vol. 76, no. 260, pp. 1743–1769, 2007.

[48] K. Cools, F. Andriulli, F. Olyslager, and E. Michielssen, "Nullspaces of MFIE and Calderon Preconditioned EFIE Operators Applied to Toroidal Surfaces," *IEEE Transactions on Antennas and Propagation*, vol. 57, no. 10, pp. 3205–3215, Oct. 2009.

[49] D. R. Wilton, "Topological consideration in surface patch and volume cell modeling of electromagnetic scatterers," in *Proc. URSI Int. Symp. Electromagn. Theory*, 1983, pp. 65–68.

[50] A. Napov and Y. Notay, "An Algebraic Multigrid Method with Guaranteed Convergence Rate," *SIAM Journal on Scientific Computing*, vol. 34, no. 2, pp. A1079–A1109, Jan. 2012.

[51] K. Cools, F. P. Andriulli, F. Olyslager, and E. Michielssen, "Improving the MFIE's accuracy by using a mixed discretization," in *2009 IEEE Antennas and Propagation Society International Symposium*, Jun. 2009, pp. 1–4.

[52] Q. Chen and D. Wilton, "Electromagnetic scattering by three-dimensional arbitrary complex material/conducting bodies," in *Antennas and Propagation Society International Symposium, 1990. AP-S. Merging Technologies for the 90's. Digest.*, May 1990, pp. 590–593 vol.2.

[53] I. Bogaert, K. Cools, F. P. Andriulli, and D. De Zutter, "Low frequency scaling of the mixed MFIE for scatterers with a non-simply connected surface," in *Electromagnetics in Advanced Applications (ICEAA), 2011 International Conference On*.   IEEE, 2011, pp. 951–954.

[54] I. Bogaert, K. Cools, F. P. Andriulli, J. Peeters, and D. De Zutter, "Low frequency stability of the mixed discretization of the MFIE," in *Antennas and Propagation (EUCAP), Proceedings of the 5th European Conference On*.   IEEE, 2011, pp. 2463–2465.

[55] R. J. Adams, "Combined field integral equation formulations for electromagnetic scattering from convex geometries," *IEEE Transactions on Antennas and Propagation*, vol. 52, no. 5, pp. 1294–1303, May 2004.

[56] O. Bruno, T. Elling, R. Paffenroth, and C. Turc, "Electromagnetic integral equations requiring small numbers of Krylov-subspace iterations," *Journal of Computational Physics*, vol. 228, no. 17, pp. 6169–6183, Sep. 2009.